Designing Bending-Active Freeform Surfaces

Emmanuel Rodriguez, Georges-Pierre Bonneau, Stefanie Hahmann, Mélina Skouras

Designing Bending-Active Freeform Surfaces

Emmanuel Rodriguez
Univ. Grenoble Alpes, Inria, CNRS, Grenoble INP, LJK
France
emmanuel.rodriguez@inria.fr

Georges-Pierre Bonneau
Univ. Grenoble Alpes, Inria, CNRS, Grenoble INP, LJK
France
georges-pierre.bonneau@inria.fr

Stefanie Hahmann
Univ. Grenoble Alpes, Inria, CNRS, Grenoble INP, LJK
France
stefanie.hahmann@inria.fr

Mélina Skouras
Univ. Grenoble Alpes, Inria, CNRS, Grenoble INP, LJK
France
melina.skouras@inria.fr

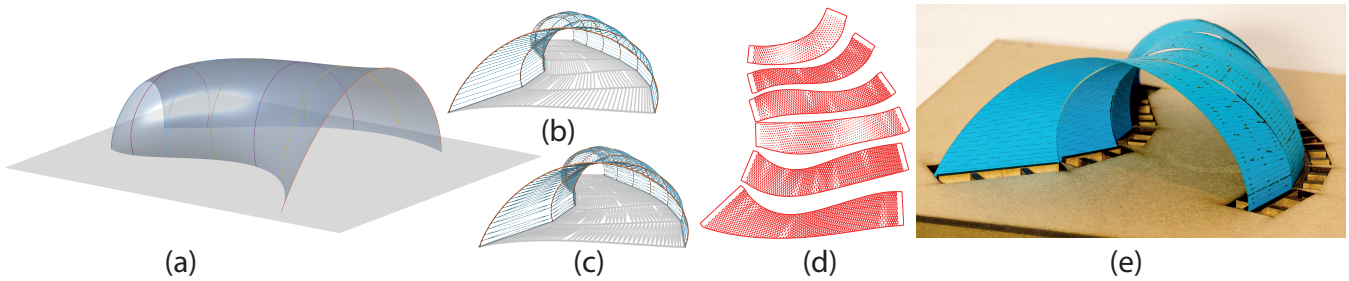

Figure 1: Overview of our method for designing architectural models made of paper strips. Given a free form input surface segmented into strips by the user (a), we first approximate the strips by developable ruled surfaces that intersect the plane along straight lines (b). We then optimize the macro-scale material properties of initially flat physical ribbons clamped at both ends such that their deformed shapes match the ruled surfaces at equilibrium (c). These material properties are converted into a dashed pattern that is added to the layout of the ribbons for laser-cutting (d). Once laser-cut, the fabricated ribbons can be actively bent to approximate the given input surface (e). Figures are high resolution, zoom in for details.

ABSTRACT

Bending-active structures are curved structures created using initially planar components that have been elastically bent so that they take on a three-dimensional shape. The 3D shape that the structure assumes depends not only on the applied external forces, but also on the elastic properties of the physical material used. By altering the fine-scale structure of this material, we are able to locally control its macroscopic elastic properties.

We introduce a computational framework for the inverse design of custom 3D surfaces using bending-active structures. We optimize the internal structure of laser-cut planar surface strips, so that they approximate a desired 3D freeform surface when being clamped at both extremities. The specific orthotropic design of the structure of the strips allows us to locally control their bending behavior. In contrast to past work the planar surface strips can be of arbitrary shape, not necessarily rectangular, and when deformed, they form a piecewise continuous surface.

SCF '24, July 07–10, 2024, Aarhus, Denmark

ACM ISBN 979-8-4007-0496-3/24/07
https://doi.org/10.1145/3639473.3665793

CCS CONCEPTS

• **Computing methodologies** → **Shape modeling**; **Computer graphics**.

KEYWORDS

active bending, homogenization, inverse design, computational fabrication, laser-cutting, shape modeling, developable ribbons

ACM Reference Format:
Emmanuel Rodriguez, Georges-Pierre Bonneau, Stefanie Hahmann, and Mélina Skouras. 2024. Designing Bending-Active Freeform Surfaces. In *ACM Symposium on Computational Fabrication (SCF '24), July 07–10, 2024, Aarhus, Denmark*. ACM, New York, NY, USA, 11 pages. https://doi.org/10.1145/3639473.3665793

1 INTRODUCTION

Cardboard is a material of choice for prototyping: it is cheap, widely available, can be cut and folded to craft models with non-trivial geometries. Inextensible but highly flexible, it can be isometrically bent to shape developable patterns. When it comes to architectural models, this decomposition into developable patches reflects that of real structures of much larger scale, including full buildings, as such patches can be easily paved with planar panels, e.g. made of glass [Liu et al. 2006]. See e.g. the remarkable work by the architects Norman Foster and Franck Gehry (Figures 2 and 8).

Here, we are interested in designing such architectural models. We assume our input is a freeform surface segmented into ribbons

by the user. Our goal is to approximate the 3D shape of the ribbons by developable surface strips made of paper or cardboard that we will clamp at both ends on a planar support.

While a multitude of 3D shapes can be formed by virtually bending the same paper strip, much fewer (generally a single one) correspond to an equilibrium state for the strip. These are the ones that minimize the elastic energy of the system. Our idea is to physically *program* the shape that each ribbon should assume by regularly laser-cutting its interior: the orientation of the cuts will force the ribbon to bend along prescribed directions (desired rulings for the 3D ribbon) while the cuts' lengths and density will allow us to control the normal curvature of the strip perpendicular to the rulings.

Rather than optimizing the sizes and positions of all the cuts independently, which would be prohibitively expensive, computationally, and numerically ill-posed, we propose a two-scale algorithm in which the cut cardboard is seen at macroscale and treated as an orthotropic *structured material*. More specifically, we first focus on characterizing the *macroscale* mechanical properties of the cardboard when laser-cut according to periodic patterns. We then solve a constrained optimization problem over these macroscale properties so that the shapes of the bent 3D ribbons at equilibrium match the desired target shapes. Finally, we map back the optimized macroscale mechanical properties to finite cuts of adequate sizes and orientations.

While this workflow is reminiscent of prior work [Rodriguez et al. 2022; Malomo et al. 2018; Chen et al. 2021], our setting presents unique challenges:

(i) Flattening arbitrary 3D strips results in planar structures which exhibit *geodesic* curvature (akin to, e.g., a piece of flat annulus), and therefore cannot be tiled using parallelograms.
(ii) Our strips have *finite* and *varying* width and have an orthotropic structure whose principle directions may be *non-orthogonal* to the "centerline" of the strip.
(iii) The intersections between developable strips and planar supports may form *curved* lines, which complexifies the fixation of the strips.

We address these challenges through our contributions:

- The novel use of a polar orthotropic laser-cut structured material family with controllable directions of orthotropy and bending stiffness;
- An algorithm to turn a given set of freeform ribbons into a set of developable ruled surfaces that can be clamped using planar pieces;
- An effective two-scale optimization method for the inverse design of developable strips that relies on a dedicated discrete ribbon model, validated with a trustful reference FEM simulator;
- The demonstration of the capabilities of our approach via the fabrication of a diverse set of physical models and their numerical analysis.

2 RELATED WORK

Paper, cardboard and other materials that come in thin plates are popular materials for the realization of mock-ups and models and have been used in various forms. Cut in planar pieces, they can serve to abstract objects' shapes [Hildebrand et al. 2012] or to build armatures [Wolff et al. 2018], or even be used for designing volumetric metamaterials [Signer et al. 2021]. While paper can be folded into complex surfaces [Kilian et al. 2008], the most common approach is to decompose the shape of the envisioned object into developable strips or patches that are bent and connected to each other to form the final structure [Mitani and Suzuki 2004; Ion et al. 2020; Massarwi et al. 2007]. This leads to a shape approximation problem that has been actively explored in the geometry processing community [Stein et al. 2018; Binninger et al. 2021; Julius et al. 2005].

Figure 2: Piecewise developable strips made of glass and steel are characteristic of the architectural style of Norman Foster. Our project aims at facilitating the design of small-scale models for this type of structures. Left: Science Center, Glasgow (photo by the authors). Right: Philological Library at FU Berlin (image from Google Earth: Google GeoBasis-DE/BKG ©2009).

In this work, we are specifically interested in the design of models for architectural vaults made of a series of arches, obtained by bending flat strips of cardboard and clamping their extremities. Rather than investigating the segmentation of the structures (that we leave up to the user to specify), we focus on the control of the 3D shape of each strip, once deformed. In this setting, physics play an important role as they determine the curvature of the strips at equilibrium. This link between geometry and mechanics has been explored by Liu et al. [2020] in the context of the design of axisymmetric structures, and later on by Hafner and Bickel [2021] and Lee et al. [2022] for more general configurations. Their respective approaches leverage straight strips whose bending rigidity is modulated by varying the width of the strips. Consequently, the resulting 3D structures exhibit large gaps and typical "staircase" profiles. In contrast, we aim at producing a C^0 approximation of the target surface when the latter is continuous. While tangential gaps can be eliminated by regularly incising the interior of the strips instead of cutting their external boundaries [Rodriguez et al. 2022; Zhang et al. 2022], gaps in the normal directions (principally due to incompatible boundary lengths for adjacent ribbons) can only be removed by using strips with an initially *curved* planar shape [Brütting et al. 2017]. We leverage these two ideas and propose a novel algorithm that approximates target freeform surfaces using regularly laser-cut strips having natural geodesic curvature. Unlike Brütting et al. who control the bending rigidity of 3D printed strips by playing with their thickness, we only rely on thick paper and a laser-cutter for fabrication, making our technique widely accessible. Another difference is that we do not assume that adjacent strips are physically connected to each other when optimizing for their parameters. While this makes the shape of our real models more

sensitive to small fabrication errors, this facilitates computation as strips can be processed independently and no assumption regarding the location of attachment points needs to be made. We note that when the target shape is well reproduced, the solution of our numerical problem is also solution of the problem with the strips attached to each other. Therefore, it is always possible to connect the strips *a posteriori* if one wants to improve the accuracy of the fabricated structures.

Unlike prior work that exploits Kirigami-inspired structures for the increased extensibility of the base material induced by the cuts [Konaković et al. 2016; Rafsanjani and Bertoldi 2017; Rafsanjani et al. 2019; Kalantar and Borhani 2018], we leverage their effect on the macro-scale *bending* stiffness of the paper. This allows us to focus on the design of piecewise developable surfaces obtained by active bending [Lienhard et al. 2013] rather than that of doubly curved shapes emerging from stretching.

In the context of architecture, active bending is also used for the construction of grid shells and their variations, i.e. deployable structures consisting in quadrilateral grids of initially planar beams, coupled via rotational joints [Mesnil 2013; Panetta et al. 2019; Pillwein et al. 2020; Suzuki et al. 2023], or for assemblies of optimized panels [Laccone et al. 2019]. Grids of bent, possibly curved, ribbons are also used for designing complex freeform surfaces through weaving [Vekhter et al. 2019; Ren et al. 2021]. However, our technique and end goal are very different from those of these lines of work. Grid shells and woven structures are used to obtain *wireframes* via the joint action of all the beams, while we produce *continuous* surfaces by manipulating individual strips. We believe our research is complementary to these works.

3 OVERVIEW

The aim of our method is to approximate a free-form surface using 3D curves extracted from the surface. The input data for our algorithm are pairs of these 3D curves representing the strips on the surface. It outputs the layouts of 2D strips that can be laser-cut. These strips are patterned with staggered cuts and approximate the input surface when they are clamped at both extremities (fixed end points and tangents). To compute the cut layouts, we propose the following pipeline:

- We approximate the input curves by a series of developable strips with shared longitudinal boundaries and intersecting the ground along rulings (Section 4). The generated strips will be used as target in our inverse design algorithm. Their unfolding to the 2D plane will define the *outer* layout of the strips to be fabricated.
- We overlay the unfolded 2D strips with a piecewise circular grid that will be used to position a parametric polar orthotropic structure whose local macroscale mechanical behavior is characterized through homogenization (Section 5).
- We optimize the lengths of each cut of the pattern using a two-scale inverse design algorithm (Section 7). For each strip, we first optimize the macroscale mechanical properties of a reduced ribbon model, described in Section 6, that approximates the behavior of the laser-cut ribbon. We then map the optimized ribbon's mechanical properties to cut lengths and generate the *internal* layout of the ribbon, formed by the cut segments (Section 8).
- We generate the layout of the support pieces, that are also laser-cut, and fabricate the final ribbon-based structure by assembling the laser cut ribbons (Section 9).

4 GENERATION OF THE 3D TARGET RIBBONS

The target surface is assumed to be segmented into strips prior to our algorithm. This section describes the algorithm for transforming these surface strips into C^0 developable ribbons by keeping the 3D curves of the surface unchanged. De facto, the developable ribbons approach the free-form input surface and thus become the *3D target ribbons* for the remaining stages of our work.

The surface strips each clamped at both extremities along straight lines are essentially 4-sided patches that have two significantly longer boundary curves and two short boarders to be clamped.

The curves segmenting the freeform are user-defined. As they are visible in the final result, we want to give the user control over their aesthetic appearance. Although the calculation of these curves is not part of our method, let's take a brief look at the advantages and disadvantages of existing methods. Such curves on the surface could be obtained in various ways, such as intersecting the shape with parallel planes, computing iso-parametric lines, surface strips from geodesic curves or paths [Liu et al. 2009; Pottmann et al. 2010; Anastas et al. 2016], paneling freeform surfaces with rectangular ribbons [Wallner et al. 2011; Kahlert et al. 2011], computing conjugate nets [Liu et al. 2006; Pottmann et al. 2008; Bauer et al. 2010], guiding by a vector field [Jakob et al. 2015], or allowing the user to draw custom curves artistically. Note, that a geodesic curve on a developable surface maps onto a straight line in the plane. This is an ideal prerequisite for computing developable strips. It is however a main feature of our method, that we do not restrict the strips to have a straight centerline, as in [Hafner and Bickel 2021; Liu et al. 2020].

Many of the methods contradict with our manufacturing specs, such as clamping the ribbons into the ground at their both ends. Geodesic curves or curvature lines may not divide surfaces into clampable strips. Conversely, arbitrarily drawn curves may be tough to interpolate with developable ribbons. Finding optimal curves balancing aesthetics, fabrication, and developability is challenging without limiting artistic expression. Displaying frame fields could guide users, but automated methods need further research. In all our examples, we use tensor product spline surfaces segmented along iso-parametric lines.

The goal now is to approximate each ribbon with a *developable ruled surface* that satisfies the following three constraints:

(A) interpolation of the long boundary curves,
(B) the clamped borders being straight line segments,
(C) the clamped borders being rulings of the developable ribbon.

The first constraint ensures the C^0-continuity of neighboring surface strips, which is an important feature of our flexible structures. The second is a manufacturing constraint for our cardboard prototypes, as it facilitates the attachment of the strips to a planar support. The third condition guarantees that all the points at the extremities of each ribbon share the same tangent plane, thus enabling the use of planar pieces for clamping the fabricated ribbons.

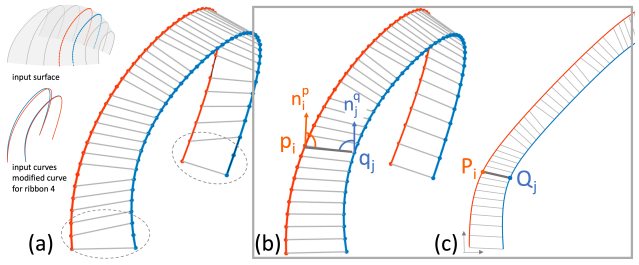

Figure 3: (a) Two curves interpolated by a planar-quad strip without constraint (C). All edges are rulings, except for the two outermost edges which are manually added. (b) Our developable strip of planar quads with edges all being rulings. (c) 2D unfolded reference state of the developable strip from (b).

As our goal is to compute a smooth developable strip that interpolates two boundary curves, a natural representation is a discrete torsal ruled surface with rulings connecting the two curves, see Fig. 3. Its rulings are either parallel (cylindrical surface), pass through a common point (conical surface), or are tangent to a curve (curve of regression), respectively. Such a discrete developable strip can be a quad strip, a triangle strip or a mix of both. A quad strip has the advantage to allow for explicit control of the singular regression curve (the loci of intersections of rulings). It is developable if only if all quads are planar, which is equivalent to the constant normal vector condition along each ruling. The limit case converges to a smooth developable strip [Pottmann et al. 2008].

Our approach works as follows. Given two 3D boundary curves with vertices $\mathbf{p} = \{\mathbf{p}_1, \ldots, \mathbf{p}_N\}$ and $\mathbf{q} = \{\mathbf{q}_1, \ldots, \mathbf{q}_M\}$, we compute a *planar-quad strip* as illustrated in Figure 3(b). This involves selecting a set of edges $(\mathbf{p}_i\mathbf{q}_j)$ as rulings that satisfy the condition

$$|\mathbf{q}_j - \mathbf{p}_i,\ \mathbf{p}'_i,\ \mathbf{q}'_j| = 0 \tag{1}$$

of developability, where $\mathbf{p}'_i, \mathbf{t}_{q_j}$ denote the tangents of the curves.

Improved tangents. The outermost edges $(\mathbf{p}_1\mathbf{q}_1)$ and $(\mathbf{p}_N\mathbf{q}_M)$ must belong to the quad strip as they will serve to clamp the surface strip to the support (constraint (B)). However, they are unlikely to be rulings. If we want them to be a ruling and the developable strip to satisfy condition (C) they must conform to equation (1). As we have n surface strips, each pair sharing a common curve between them, our goal is to perturb the $n+1$ curves as little as possible while guaranteeing that the new tangent vectors at the ends of the curves satisfy (1) for each strip. To solve this problem for the n strips simultaneously, we proceed in two steps. We first compute optimal tangent vectors for all curves' endpoints and then perturb the curves smoothly so that they interpolate the optimal tangents.

Let $\mathbf{x}_i$ denote the first point of curve i and $\mathbf{t}_i$ the first tangent vector of curve i, $(i = 1 \ldots, n+1)$, as illustrated in Figure 4. Our algorithm is based on the following insight: For each strip i, the vectors $\mathbf{x}_i - \mathbf{x}_{i-1}, \mathbf{t}_{i-1}, \mathbf{t}_i$ satisfying (1) span a plane, which is the constant tangent plane Π_{i-1} along the ruling $(\mathbf{x}_{i-1}\mathbf{x}_i)$. See Fig. 4 for notations. When (1) is satisfied for all strips, it follows that the new tangent vectors $\mathbf{t}_i$ lie respectively at the intersection $\Pi_{i-1} \cap \Pi_i$.

Our idea is therefore to find the best n tangent planes, so that the tangent vectors $\tilde{\mathbf{t}}_i$ at the intersection minimize $||(\tilde{\mathbf{t}}_1, \ldots, \tilde{\mathbf{t}}_n) - (\mathbf{t}_1, \ldots, \mathbf{t}_n)||^2$. To do this, we consider a vector $\mathbf{u}_i$ which together with $(\mathbf{x}_i - \mathbf{x}_{i-1})$ spans the tangent plane Π_i. We then define a function $F(\mathbf{u}_1, \ldots, \mathbf{u}_n) = (\bar{\mathbf{t}}_1, \ldots, \bar{\mathbf{t}}_n)$, that maps any n vectors $(\mathbf{u}_1, \ldots, \mathbf{u}_n)$ to $n+1$ tangent vectors satisfying (1) and solve the problem:

$$(\tilde{\mathbf{u}}_1, \ldots, \tilde{\mathbf{u}}_n) = \text{argmin}\ ||F(\mathbf{u}_1, \ldots, \mathbf{u}_n) - (\mathbf{t}_1, \ldots, \mathbf{t}_n)||^2. \tag{2}$$

F is defined as follows: Let $\mathbf{v}_i = (\mathbf{x}_{i+1} - \mathbf{x}_i) \times \mathbf{u}_i$, $i = 2, \ldots, n$ then

$\bar{\mathbf{t}}_i \in \mathbf{v}_{i-1}^{\perp} \cap \mathbf{v}_i^{\perp}$ and $||\bar{\mathbf{t}}_i|| = ||\mathbf{t}_i||$ (intersection of planes)
$\bar{\mathbf{t}}_1$ = orthogonal projection of $\mathbf{t}_i$ onto the plane $\mathbf{v}_1^{\perp}$
$\bar{\mathbf{t}}_n$ = orthogonal projection of $\mathbf{t}_n$ onto the plane $\mathbf{v}_n^{\perp}$.

We solve the small non-linear least-square problem (2) using Scipy-optimize. In conclusion, the improved tangents $\tilde{\mathbf{t}}_i$ guarantee that the first edge $x_{i+1} - x_i$ of strip i (for all i) is indeed a ruling. The same procedure is applied to the other border of the strips. We finally compute a new smooth curve $\tilde{\mathbf{p}}$ by solving the linear problem

$$\tilde{\mathbf{p}} = \min ||\tilde{\mathbf{p}} - \mathbf{p}||^2 + \omega||\tilde{\mathbf{p}}'' - \mathbf{p}''||^2 \text{ s.t. } \tilde{\mathbf{t}}_1 = \mathbf{t}_1 \text{ and } \tilde{t}_N = t_N. \tag{3}$$

A comparison of quad strips is shown in Fig. 3 with improved tangents in (b) without in (a). The big quads at the borders are due to bad rulings. The inset in (a) compares the curves before and after tangent modification.

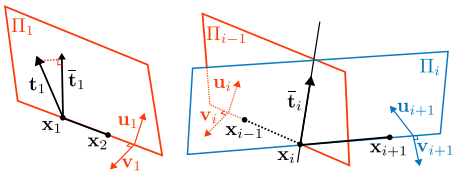

Figure 4: Improvement of tangents in order to transform the outermost edges to rulings of the developable strip.

Computation of planar quad strip. Most algorithms for computing developable strips result in triangle strips [Wang and Tang 2005; Liu et al. 2009; Massarwi et al. 2008; Liu et al. 2011]. The PQ strip method of [Liu et al. 2006] would be suitable for our task, but requires an initial guess of a quad strip being close to be developable. As we cannot guarantee this, we implemented a modified version of the algorithm from [Wang and Tang 2005] which uses triangles only to accord to a planar quad strip. It is a dynamic programming approach which maps the rulings to a directed acyclic graph and computes the optimal sequence of rulings as a shortest path. Unlike the approach taken in [Wang and Tang 2005], we design the graph to ensure that no pair of rulings shares the same curve point, resulting in a quad strip rather than a triangle strip. The optimality criterion (weights in the graph) reflects the constant tangent plane condition (1) of the rulings in terms of normal vectors by defining for a transverse edge $(\mathbf{p}_k\mathbf{q}_l)$ the *normal twist* $T(k,l) = 1 - \mathbf{n}_{p_k} \cdot \mathbf{n}_{q_l}$, where $\mathbf{n}$ is the unit normal vector at the corresponding vertex.

The optimal sequence of edges minimizes the sum of normal twists as a measure of developability. Specifically, when $\sum T(k,l) = 0$, the edges $(\mathbf{p}_k\mathbf{q}_l)$ represent the rulings of a developable strip, and equivalently, all quads become planar. Fig. 3 shows an example, in

(b) the planar-quad strip and in (c) its 2D planar state after unfolding to a plane.

Each strip element is bounded by two transverse edges, the rulings, connecting points of **p** and **q**, and two curves coinciding with one or possibly more curve segments of either **p** and **q**, e.g. see the quads in Figure (b) based on 5 curve points instead of 4.

5 INTERNAL STRUCTURE DESIGN

The shape of our target developable strips can be characterized by their shape in their flattened state, the direction of the rulings and the normal curvature in the direction orthogonal to the rulings. To favor bending of the fabricated ribbons in this direction, we decrease their bending rigidity in this particular direction by patterning them with an orthotropic laser-cut mesostructure formed by straight segments aligned with the rulings and arranged in staggered rows (see Figure 5). In our discrete setting, the cuts of the ribbons are positioned on piecewise circular grids defined between successive rulings of the unfolded strips. The spacing between the radial lines of the circular grid of each ribbon piece is uniform and set by prescribing the length L_{min} of the arched side of the narrower cells of the grid. The offset between circular lines is constant and set to a prescribed value $T/2$. We locally parametrize the cutting pattern by the distance L between successive rows of cuts, T the distance between the centers of adjacent cuts in the radial direction, and t the length of the cuts. Note that L and t are spatially varying quantities, while T is kept fixed. Here, we set $L_{min} = 2$ mm and $T = 1$ cm.

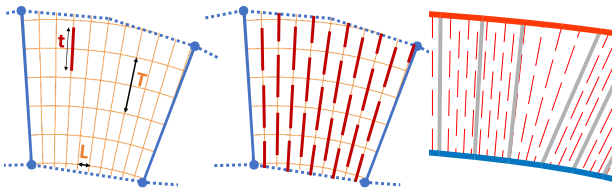

Figure 5: Positioning of orthotropic laser-cuts (red strokes) on an individual polar grid defined on each quad strip element (left). Piecewise continuous pattern (right).

Carboard cut this way behaves as an orthotropic material, but the pattern is not periodic. Therefore, we cannot characterize its mechanical behavior using homogenization straight away. Since our ribbons do not exhibit any tangential bending or stretching, and that geodesic curvature is relatively small compared to the spacing between the cuts rows, we hypothesize that geodesic curvature do not play an important role in our case, and we approximate mechanical properties at a given point by locally unwarping the grid so that it takes a rectangular shape, which allows us to recover the setting in which standard homogenization techniques apply.

To estimate the bending stiffness of the unwarped structured material perpendicularly to the cuts, we follow the homogenization-based approach of Rodriguez et al. [2022] that matches the elastic energy of a periodic metamaterial under flexion to that of a 2D Kirchhoff rod with rectangular cross-section and energy density (per unit length) $\frac{1}{2}k_b W\kappa^2$, with W the width of the rod and κ its local curvature in the 2D plane. However, here, instead of using a

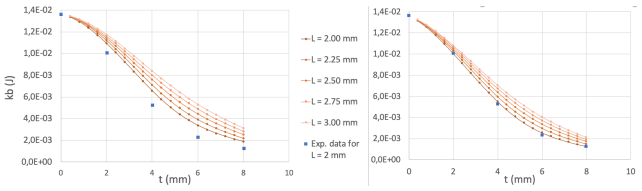

Figure 6: Left: Bending stiffnesses of our laser-cut structured material perpendicularly to the cuts, as originally computed using our homogenization approach, and without accounting for the modification of the material properties induced by the laser cutting process. Right: Rescaled bending stiffnesses using the rightmost measured data point to compensate for the latter effect. Blue squares represent stiffnesses experimentally measured.

volume representation for the reference fine-scale model, we rely on a much faster Naghdi's plate model [Naghdi 1962]. In practice, we use the numerical simulation package FEnicCS [Hale et al. 2018] to carry out all reference simulations using meshes of about 50k vertices for domains consisting in 2×2 periodic tiles.

Figure 6 (left) shows the obtained homogenized bending stiffnesses for the range of (L, t) parameters used in this work (the width of the cuts is kept fixed and set to the width of the laser line, here 0.27 mm). When compared to experimental values of k_b (blue square markers in the figure), obtained from cantilever tests performed as advised by Romero et al. [2021], we observe a good agreement in the "shape" of our curves but non-negligible differences in terms of absolute values. We attribute this error to local modifications of the mechanical properties of the paper due to "burning" in the vicinity of the areas cut by the laser. To verify this hypothesis we conducted cantilever tests with three laser-cut rectangles (without incisions) of same length 350 mm and respective widths 20 mm, 5 mm and 2 mm, as shown in the inset figure. Here the laser-cutting process burns the sides of the ribbons. As a result the deflection increases for ribbons of decreasing widths, showing that the paper becomes softer when the relative area of burnt paper increases. We leave as future work the proper modeling of the physical phenomena at play, and account for this effect by linearly rescaling our computed stiffnesses using the experimental value corresponding to paper with the longest cuts ($t = 8$ mm, $L = 2$ mm). The rescaled bending stiffnesses k_b are shown in Figure 6 (right).

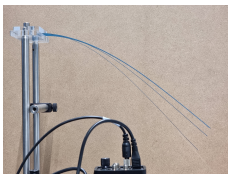

6 REDUCED MODEL

The 2D Kirchhoff rod model used in the previous section, and its discretization based on a 2D discrete elastic rod [Bergou et al. 2008], allows us to efficiently approximate the behavior of an inextensible orthotropic 3D ribbon that is straight at rest, that bends perpendicularly to its centerline, and whose material properties may vary longitudinally. We now seek a generalization of this model that

could be used for our specific application. First, our discrete reduced model should support ribbons with natural geodesic curvature. Second, it should allow flexion of the ribbons in tilted directions. In order to enlarge our design space, we also want the material properties of the ribbons to be able to (linearly) vary, transversely. Finally, it should be fast and robust so that it can be used effectively in an inverse design algorithm. While the 3D version of discrete elastic rods can be used to model ribbons that exhibit natural curvature in their tangent plane (although their accuracy for wide ribbons is debatable [Charrondière et al. 2020]), we are not aware of any extension that would also fulfill the other requirements. In particular, 3D Discrete Elastic Rods [Bergou et al. 2008] cannot be used to model the behavior of ribbons whose directions of material orthotropy are not perpendicular to the centerline of the rod.

Since our reduced model is intended to be used for (quasi) inextensible ribbons made of a material whose bending stiffness is much weaker in one direction, we assume that the directions of flexion are known a priori and match the directions of the cuts, and we restrict possible bending to these directions.

To satisfy all our requirements, we propose to model ribbons as mass-spring networks formed by both linear and angular springs, built from the discretized strips described in Section 4. We arrange the springs in the networks so that they well represent the finite geometry of the ribbons and their non-orthogonal bending directions. Each element of the strip is assumed to be rigid so that motion is restricted to flexion about the strip's transverse edges. We model this behavior by connecting the 4 corners of each strip element using 6 springs (4 springs are used to connect adjacent corners while 2 springs connect corners diagonally), as illustrated in Figure 7-top. Isometric deformations are enforced by assigning a high stiffness value to these springs. In practice, we did not experience slow convergence due to this simple way of enforcing constant length, and we found it sufficient in our case as ribbons that bend typically do not want to stretch nor compress so that this constraint did not need to be fought very hardly. We will denote by E_s the total stretching energy of these springs.

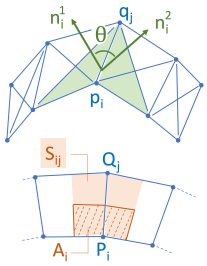

Figure 7: Reduced model.

With this arrangement of springs, bending is only permitted about the transverse edges. We model the bending energy associated to such edge (P_iQ_j) connecting vertices P_i to Q_j as a function of the normal curvature κ perpendicular to the edge

$$E_b^{ij} = \int_{S_{ij}} \frac{1}{2} k_b \kappa^2 dS, \tag{4}$$

where S_{ij} is the domain associated to edge (P_iQ_j). This formulation of the bending energy, that explicitly depends on the varying curvature along the edge is what allows us to account for conical curvature of the ribbon even if we locally unwarp our structured material.

Inspired by the formulation used in Discrete Elastic Rods [Bergou et al. 2008] for defining discrete normal curvatures, we discretize the above energy using two integration points as

$$E_b^{ij} \approx \frac{1}{2} k_i (\frac{\kappa_i}{L_i})^2 A_i + \frac{1}{2} k_j (\frac{\kappa_j}{L_j})^2 A_j, \tag{5}$$

where k_i (resp. k_j) denotes the bending stiffness at vertex $\mathbf{P}_i$ (resp. $\mathbf{Q}_j$), κ_i (resp. κ_j) the discrete normal curvature integrated along the longitudinal direction of the domain S_{ij} associated to vertex $\mathbf{P}_i$ (resp. $\mathbf{Q}_j$), A_i (resp. A_j), the Voronoi area of vertex $\mathbf{P}_i$ (resp. $\mathbf{Q}_j$), and L_i (resp. L_j) the size of the domain in the longitudinal direction that we define as $L_i = \frac{A_i}{||P_i - Q_j||/2}$ (resp. $L_j = \frac{A_j}{||P_i - Q_j||/2}$).

We estimate the integrated curvature κ_i, using the norm of the discrete curvature binormal

$$(\kappa \mathbf{b})_i = \frac{\mathbf{n}_i^1 \times \mathbf{n}_i^2}{|\mathbf{N}_i^1||\mathbf{N}_i^2| + \mathbf{n}_i^1 \cdot \mathbf{n}_i^2}, \tag{6}$$

where $\mathbf{n}_i^1$ and $\mathbf{n}_i^2$ are the current area-weighted normals of the triangles incident to edge $(\mathbf{p}_i\mathbf{q}_j)$ containing $\mathbf{p}_i$, and $\mathbf{N}_i^1$ and $\mathbf{N}_i^2$ their counterparts in the reference configuration (see Figure 7). We proceed similarly for computing κ_j. Note that this binormal vector has norm $2\tan(\theta/2)$ with θ the angle between $\mathbf{n}_i^1$ and $\mathbf{n}_i^2$ and that the *integrated* curvatures κ_i and κ_j should agree, up to small mismatches in the normals computed at vertices $\mathbf{p}_i$ and $\mathbf{q}_j$ due to our use of a soft penalty term to enforce isometry.

We will denote by E_b the total bending energy of the ribbon.

Finally, we account for the effect of gravity on the system by lumping the mass of each section S_{ij} of the ribbon associated to edge e to its two end vertices $\mathbf{P}_i$ and $\mathbf{Q}_j$, i.e we assign a mass $m_i = \rho A_i$ (resp. $m_j = \rho A_j$) to the vertex $\mathbf{P}_i$ (resp. $\mathbf{Q}_j$), with ρ denoting the areal density of the paper. We can then define the corresponding gravitational energy as

$$E_g^{ij} = m_i g z_i + m_j g z_j \tag{7}$$

where g is the constant of gravity and z_i (resp. z_j) the vertical coordinate of point $\mathbf{p}_i$ (resp. $\mathbf{q}_j$). Note that, here, we neglected the mass deficit due to the presence of cuts, given their small width (0.27 mm) compared to the spacing between the cut rows (between 2 mm and 3 mm). The total gravitational energy is denoted by E_g.

The shape of the ribbon at equilibrium can be obtained by minimizing its total energy $E = E_s + E_b + E_g$ with respect to the positions in the current configuration of the vertices of all its transverse edges (p_iq_j).

7 INVERSE DESIGN ALGORITHM

Given a 3D target quad strip whose vertices positions are denoted by $\hat{\mathbf{p}}$ and $\hat{\mathbf{q}}$, stacked in a vector $\hat{\mathbf{x}} = (\hat{\mathbf{p}}, \hat{\mathbf{q}})$, and its unfolding $\mathbf{X} = (\mathbf{P}, \mathbf{Q})$, we are now looking to optimize the bending stiffnesses k_b of the associated physical ribbon so that the shape of the ribbon at equilibrium, when clamped at its extremities, matches that of the target strip. The optimized bending stiffnesses will be converted into a lasercut pattern in a subsequent stage.

Letting $\mathbf{x} = (\mathbf{p}, \mathbf{q})$ denote the positions of the nodes of the discrete ribbon, we cast our problem as

$$\min_{\mathbf{x}, k_b} \Phi(\mathbf{x}, \hat{\mathbf{x}}, k_b) \text{ s.t. } \frac{\partial E(\mathbf{x}, k_b)}{\partial \mathbf{x}} = 0 \text{ and } k_{min} \leq k_b \leq k_{max}, \tag{8}$$

where Φ is a cost function (whose terms are detailed below) penalizing the deviation of the ribbon's deformed shape from its desired

target shape and the nonlinear constraints impose the forces acting on the ribbon to cancel out, i.e. enforce the static equilibrium of the ribbon.

Clamping. We model clamping of the ribbon at its extremities by extending the ribbon by one quad at both ends and fixing the positions of the four nodes of each of the two extra quads. We define the positions of these nodes such that they lie in the tangent planes of their respective adjacent quads in the target configuration. These positions are treated as hard constraints when solving the minimization problem (8).

Cost function. Let I_1, resp. I_2, denote the indices of the vertices in $\mathbf{x}$ corresponding to the points $\mathbf{p}$ (resp. $\mathbf{q}$). We define the cost function Φ as the sum of three terms Φ_{shape}, Φ_{dist} and Φ_{reg} described below.

$$\Phi_{shape}(\mathbf{x}, \hat{\mathbf{x}}) = \sum_{j=1}^{2} \sum_{i \in I_j} (||\mathbf{c}(\mathbf{x}_i) - \mathbf{c}(\hat{\mathbf{x}}_i)||^2), \tag{9}$$

with $\mathbf{c}(\mathbf{x}_i) = (\mathbf{x}_{i+1} - 2\mathbf{x}_i + \mathbf{x}_{i-1})$, penalizes differences in shapes between the boundaries of the current and target ribbons, defined in terms of local curvature, an effective shape descriptor from a perceptual point of view [Arkin et al. 1990]. Note that, here, this term principally captures differences in *normal* curvature since the two ribbons have same metric.

$$\Phi_{dist}(\mathbf{x}, \hat{\mathbf{x}}) = \sum_{j=1}^{2} \sum_{i \in I_j} (||\mathbf{x}_i - \hat{\mathbf{x}}_i||^2) \tag{10}$$

penalizes the vertex-wise L_2 distance between the points of the current and target ribbons. We use this term to prevent shift of the ribbon or rotation of parts of the ribbon with low curvature.

$$\Phi_{reg}(k_b) = \sum_{j=1}^{2} \sum_{i \in I_j} (|k_{i+1} - 2k_i + k_{i-1}|^2) \tag{11}$$

acts as a regularizer, smoothing out the nodal bending stiffnesses along either ribbon boundary.

Stiffnesses bounds. The bounds on the admissible bending stiffnesses k_b relate to fabrication constraints and depend on the local spacing between the radial lines of the cutting layout pattern. Thus the bounds are different for each component of k_b. We set them by first creating the piecewise circular grid used to position the cuts on the unfolded strip $\mathbf{X}$ (see Figure 5), then reading the L value corresponding to each vertex $\mathbf{X}_i$ of the strip, and finally looking for the minimum and maximum k_b corresponding to this L in our table mapping the cut parameters (L, t) to stiffnesses k_b (see Section 5).

We solve problem (8) with the minimization library IPOPT [Wächter et al. 2002], using its quasi-Newton BFGS implementation. We initialize each component of k_b with the value corresponding to plain paper, and the vertex positions $\mathbf{x}$ with the values corresponding to the static equilibrium of the ribbon obtained by minimizing the energy E starting from the target positions $\hat{\mathbf{x}}$.

8 MAPPING BENDING STIFFNESSES TO CUTS PARAMETERS

The final step of our pipeline consists in generating a dashed pattern from the optimized bending stiffnesses k_b. Since the relation between the cuts lengths t and the bending stiffnesses k_b is monotonic for a given spacing value L (see Figure 5), we can easily invert the piecewise linear function $k_b = f(t; L)$ by reflecting the graph of the function over the line $k_b = t$. We can then convert the computed nodal k_b to cut lengths t by bilinear interpolation of the (t, L) values of the inverse maps. Finally, for each vertex of the circular pattern grid corresponding to a cut, we deduce the cut length from the values at the corners of the belonging quad using again bilinear interpolation.

9 RESULTS

We validated our approach by using our algorithm to design four different surfaces of various shapes (cocoon, asymmetric tent, leaning tent, tunnel), that we also fabricated. These surfaces consist in a total of 23 ribbons and exhibit various features, including highly curved areas (asymmetric and leaning tents, cocoon) and areas with negative Gaussian curvature (tunnel). The planar ribbons can have highly curved boundaries, with multiple curvature maxima. The direction as well as the density of the cuts show large variations. The results are shown in Figures 9 and 10. See also the accompanying video. It is possible to visually match regions of high cut's density in the planar ribbons, corresponding to low value of the stiffnesses, with highly curved regions on the surfaces.

Fabrication. We use a 260 g m^{-2} paper for fabricating our ribbons. This paper comes in 70 × 50 cm plates that are 0.34 mm thick. Our physical models are about 20x20x15 cm^3 which corresponds to strips of 20 to 30 cm long, and 2 to 3 cm width. The Young's modulus of the paper was experimentally estimated to 3.79 GPa from a cantilever test. The planar support and the fixation pieces are laser-cut in a 3 mm thick mdf wood, those shapes are specifically designed to constrain the tangents of the ribbons at their extremities (See Figure 10).

As we can see in Figure 10, the shapes of the fabricated models agree well, visually, with the piecewise developable target surfaces, despite remaining minor gaps (less than 3 mm) that we explain in part to fabrication tolerances and variations in material properties of the paper. We confirmed this sensibility to small fabrication errors by fabricating 6 times a same ribbon and observing some variability. We further assessed the approximation quality of our algorithm by conducting numerical experiments and comparing our results with that obtained using a trustful reference simulator.

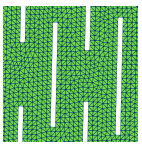

Numerical analysis. We used the FEniCS implementation of Naghdi's plate model for generating our fine-scale references. We set the size of the elements to 0.3 mm, which results in meshes with 150k to 220k triangles, as illustrated in the inset figure. Simulation time for the reference fine-scale is slightly less than 30mn for each ribbon, on a 16 core Intel Xeon 3433 workstation.

A visual comparison between the target developable planar quad strips (row (a) in Fig. 9) and the solution of the inverse design problem (8) (position $\mathbf{x}$ in row (c), stiffnesses k_b in row (b)) suggests a good match, which is confirmed by the numerical results in the two left-most columns of Table (1). Crucially the Hausdorff distance visualizations (row (d)) between the reference simulation of the cut ribbons, constructed from the stiffnesses solution of the inverse problem (8), and the reduced model with the same stiffnesses (row (c)), reveal a remarkably small error, **confirming the validity of our reduced model (Section 6)**, see also the statistics of the Hausdorff distances in Table (1). To further analyze our algorithm, we computed the equilibrium shapes of our reduced model, with the same ruling directions and with - non-optimal - constant stiffnesses, corresponding to the Young's modulus of the paper (row (e)). The poor shape correspondence with the target quad strips (row (a)) emphasizes the impact of the length of the cuts, not only their directions. The importance of the direction of the cuts is revealed by comparing these latter results with the reference fine-scale simulation of solid paper (row (f)), for which the direction of bending is not constrained. Finally, comparing the poor matching between the reference simulation of uncut ribbons (row (f)) and the target developable quad strip (row (a)) with the quality of the match for the cut ribbons, as revealed in the Hausdorff visualizations (row (d)), further underlines the interest of our algorithm.

Timings. Computing the planar quad strips takes on average 4s per ribbon, with a non-optimized Matlab implementation. Most of the time is spent on the inverse modeling for computing the stiffnesses (equation (8) Section 7). Here the timings vary from 48s for the 5 ribbons of the Cocoon example, to 3mn30s for the 6 ribbons of the tunnel example, with an average of 30s per ribbon.

Table 1: For each of the 4 examples in Figure 9, from left to right called cocoon, asymmetric tent, leaning tent, tunnel, we report the average and maximum deviation for numerical validation. D_c denotes the absolute L_2-distance in mm between boundary curves of resulting ribbons and target ribbons. D_s measures the Hausdorff-distance between the reference fine-scale simulation of mesostructured ribbons and the simulation with our reduced model from Section 6. Absolute distances are given in mm, relative distance with respect to the bounding-box diagonal length. Timings are given in the text.

models	abs. D_c mm	rel. D_c	abs. avrD_s mm	abs. maxD_s mm	rel. avrD_s	rel. maxD_s
cocoon	0.17	0.000	1.3	6.1	0.005	0.02
asym. tent	0.18	0.000	0.4	2.1	0.002	0.008
leaning tent	0.32	0.001	0.7	4.0	0.002	0.015
tunnel	1.55	0.006	0.2	1.1	0.001	0.004

10 CONCLUSION

We have presented a method for the computational design of freeform surfaces formed by bending-active strips and explored its application to the fabrication of architectural prototypes. As demonstrated by our examples, our method proved effective in practice. However, it has some limitations that leave avenues for future work. For example, our inverse design algorithm only takes smooth developable ruled surfaces as input, while some buildings exhibit sharp edges (see Figure 8-left for an example). Others are made of closed strips (Figure 8-right), while we only consider ribbons touching the ground. Generalizing our method to handle such features (and see how we could fabricate them in practice) would be an interesting extension. We also limited our evaluation to ribbons whose dihedral angles after discretization are all positive. Fully exploring the design space of ribbons with geodesic curvature and their possible "inflections", as done by Hafner and Bickel [2021] for the case of straight ribbons, would be valuable. Finally, we only considered structures touching a common planar support, which eases fabrication. While our inverse design algorithm can already be used in some cases that do not satisfy this requirement (see our Lamp example in Figure 10(e)), working on more complex boundary conditions would open up the potential applications. See, e.g. Figure 8-bottom for an extremely challenging, but very exciting, configuration.

Figure 8: Left: SEC Armadillo, Glasgow (photo by Adrian Pingstone, Wikimedia Commons, public domain). Right: City Hall London by Norman Foster (photo by StaraBlazkova, Wikimedia Commons, CC BY-SA 3.0). Bottom: Jay Pritzker Pavilion by Frank Gehry (photo by Sea Cow, Wikimedia Commons, CC BY-SA 4.0).

ACKNOWLEDGMENTS

This work was supported by the European Union's Horizon 2020 programme under grant agreement No 862025 (FETOpen *ADAM*^{2}) and the Alexander von Humboldt Foundation. The authors would like to thank Victor Romero for his help with material measurements, Laurence Boissieux for having edited our video, and Stan Borkowski for assistance with the laser-cutting machine.

REFERENCES

Yousef Anastas, Michelle Gillet, L. Rowenczyn, and Olivier Baverel. 2016. Complex Surface Approximation with Developable Strips. *Journal of the International Association for Shell and Spatial Structures* 57 (06 2016), 133–143. https://doi.org/10.20898/j.iass.2016.188.732

Esther M. Arkin, L. Paul Chew, Daniel P. Huttenlocher, Klara Kedem, and Joseph B. M. Mitchell. 1990. An efficiently computable metric for comparing polygonal shapes.

IEEE Trans. Pattern Anal. Mach. Intell. 13 (1990), 209–216.

Ulrich Bauer, Konrad Polthier, and Max Wardetzky. 2010. Uniform Convergence of Discrete Curvatures from Nets of Curvature Lines. *Discrete and Computational Geometry* 43, 4 (2010), 798–823.

Miklós Bergou, Max Wardetzky, Stephen Robinson, Basile Audoly, and Eitan Grinspun. 2008. Discrete elastic rods. In *ACM SIGGRAPH 2008 Papers* (Los Angeles, California) *(SIGGRAPH '08)*. Association for Computing Machinery, New York, NY, USA, Article 63, 12 pages. https://doi.org/10.1145/1399504.1360662

Alexandre Binninger, Floor Verhoeven, Philipp Herholz, and Olga Sorkine-Hornung. 2021. Developable Approximation via Gauss Image Thinning. *Computer Graphics Forum* 40, 5 (2021), 289–300. https://doi.org/10.1111/cgf.14374

Jan Brütting, Axel Körner, Daniel Sonntag, and Jan Knippers. 2017. Bending-Active Segmented Shells. In *Proceedings of the IASS annual symposium*.

Raphaël Charrondière, Florence Bertails-Descoubes, Sébastien Neukirch, and Victor Romero. 2020. Numerical modeling of inextensible elastic ribbons with curvature-based elements. *Computer Methods in Applied Mechanics and Engineering* 364 (2020), 112922. https://doi.org/10.1016/j.cma.2020.112922

Tian Chen, Julian Panetta, Max Schnaubelt, and Mark Pauly. 2021. Bistable auxetic surface structures. *ACM Trans. Graph.* 40, 4 (2021). https://doi.org/10.1145/3450626.3459940

Christian Hafner and Bernd Bickel. 2021. The Design Space of Plane Elastic Curves. *ACM Trans. Graph.* 40, 4, Article 126 (jul 2021), 20 pages. https://doi.org/10.1145/3450626.3459800

Jack S. Hale, Matteo Brunetti, Stéphane P.A. Bordas, and Corrado Maurini. 2018. Simple and extensible plate and shell finite element models through automatic code generation tools. *Computers & Structures* 209 (2018), 163–181. https://doi.org/10.1016/j.compstruc.2018.08.001

Kristian Hildebrand, Bernd Bickel, and Marc Alexa. 2012. crdbrd: Shape Fabrication by Sliding Planar Slices. *Computer Graphics Forum* 31, 2pt3 (2012), 583–592. https://doi.org/10.1111/j.1467-8659.2012.03037.x

Alexandra Ion, Michael Rabinovich, Philipp Herholz, and Olga Sorkine-Hornung. 2020. Shape Approximation by Developable Wrapping. *ACM Trans. Graph.* 39, 6, Article 200 (nov 2020), 12 pages. https://doi.org/10.1145/3414685.3417835

Wenzel Jakob, Marco Tarini, Daniele Panozzo, and Olga Sorkine-Hornung. 2015. Instant field-aligned meshes. *ACM Trans. Graph.* 34, 6, Article 189 (nov 2015), 15 pages. https://doi.org/10.1145/2816795.2818078

Dan Julius, Vladislav Kraevoy, and Alla Sheffer. 2005. D-Charts: Quasi-Developable Mesh Segmentation. *Computer Graphics Forum* (2005). https://doi.org/10.1111/j.1467-8659.2005.00883.x

Joe Kahlert, Matt Olson, and Hao Zhang. 2011. Width-bounded geodesic strips for surface tiling. *Visual Computer* 27, 1 (jan 2011), 45–56. https://doi.org/10.1007/s00371-010-0513-3

Negar Kalantar and Alireza Borhani. 2018. Informing Deformable Formworks - Parameterizing Deformation Behavior of a Non-Stretchable Membrane via Kerfing. In *Learning, Adapting and Prototyping - Proceedings of the 23rd CAADRIA Conference - Volume 2, Tsinghua University, Beijing, China, 17-19 May 2018, pp. 339-348.*

Martin Kilian, Simon Flöry, Zhonggui Chen, Niloy J. Mitra, Alla Sheffer, and Helmut Pottmann. 2008. Curved Folding. *ACM Trans. Graph.* 27, 3 (aug 2008), 1–9. https://doi.org/10.1145/1360612.1360674

Mina Konaković, Keenan Crane, Bailin Deng, Sofien Bouaziz, Daniel Piker, and Mark Pauly. 2016. Beyond Developable: Computational Design and Fabrication with Auxetic Materials. *ACM Trans. Graph.* 35, 4 (2016). https://doi.org/10.1145/2897824.2925944

Francesco Laccone, Luigi Malomo, Jesus Pérez, Nico Pietroni, Federico Ponchio, Bernd Bickel, and Paolo Cignoni. 2019. FlexMaps Pavilion: a twisted arc made of mesostructured flat flexible panels. *Proceedings of IASS Ann. Symposia* 2019, 5 (2019), 1–7.

Ting-Uei Lee, Joseph M. Gattas, and Yi Min Xie. 2022. Bending-active kirigami. *International Journal of Solids and Structures* 254-255 (2022), 111864. https://doi.org/10.1016/j.ijsolstr.2022.111864

Julian Lienhard, Holger Alpermann, Christoph Gengnagel, and Jan Knippers. 2013. Active Bending, a Review on Structures where Bending is Used as a Self-Formation Process. *International Journal of Space Structures* 28, 3-4 (2013). https://doi.org/10.1260/0266-3511.28.3-4.187

Mingchao Liu, Lucie Domino, and Dominic Vella. 2020. Tapered elasticæ as a route for axisymmetric morphing structures. *Soft Matter* 16 (2020). Issue 33. https://doi.org/10.1039/D0SM00714E

Yang Liu, Helmut Pottmann, Johannes Wallner, Yong-Liang Yang, and Wenping Wang. 2006. Geometric modeling with Conical meshes and Developable Surfaces. *ACM Trans. Graph.* 25, 3 (jul 2006), 681–689. https://doi.org/10.1145/1141911.1141941

Yong-Jin Liu, Yu-Kun Lai, and Shimin Hu. 2009. Stripification of Free-Form Surfaces With Global Error Bounds for Developable Approximation. *IEEE Transactions on Automation Science and Engineering* 6, 4 (2009), 700–709. https://doi.org/10.1109/TASE.2008.2009926

Yong-Jin Liu, Kai Tang, Wen-Yong Gong, and Tie-Ru Wu. 2011. Industrial design using interpolatory discrete developable surfaces. *Computer-Aided Design* 43, 9 (2011), 1089–1098. https://doi.org/10.1016/j.cad.2011.06.001

Luigi Malomo, Jesús Pérez, Emmanuel Iarussi, Nico Pietroni, Eder Miguel, Paolo Cignoni, and Bernd Bickel. 2018. FlexMaps: Computational Design of Flat Flexible Shells for Shaping 3D Objects. *ACM Trans. Graph.* 37, 6 (2018). https://doi.org/10.1145/3272127.3275076

Fady Massarwi, Craig Gotsman, and Gershon Elber. 2007. Papercraft Models using Generalized Cylinders. In *15th Pacific Conference on Computer Graphics and Applications (PG'07)*. https://doi.org/10.1109/PG.2007.16

Fady Massarwi, Craig Gotsman, and Gershon Elber. 2008. Paper-craft from 3D polygonal models using generalized cylinders. *Computer Aided Geometric Design* 25, 8 (2008), 576–591. https://doi.org/10.1016/j.cagd.2008.06.007 Computer Graphics and Applications.

Romain Mesnil. 2013. Stability of elastic gridshells. *Thesis dissertation* (06 2013). https://doi.org/10.13140/RG.2.1.1727.3449

Jun Mitani and Hiromasa Suzuki. 2004. Making Papercraft Toys from Meshes Using Strip-Based Approximate Unfolding. *ACM Trans. Graph.* 23, 3 (2004). https://doi.org/10.1145/1015706.1015711

P. M. Naghdi. 1962. Foundations of elastic shell theory. *Berkeley: Institute of Engineering Research, University of California.* (1962).

J. Panetta, M. Konaković-Luković, F. Isvoranu, E. Bouleau, and M. Pauly. 2019. X-Shells: A New Class of Deployable Beam Structures. *ACM Trans. Graph.* 38, 4, Article 83 (jul 2019), 15 pages. https://doi.org/10.1145/3306346.3323040

Stefan Pillwein, Kurt Leimer, Michael Birsak, and Przemyslaw Musialski. 2020. On Elastic Geodesic Grids and Their Planar to Spatial Deployment. *ACM Trans. Graph.* 39, 4 (2020). https://doi.org/10.1145/3386569.3392490

Helmut Pottmann, Qixing Huang, Bailin Deng, Alexander Schiftner, Martin Kilian, Leonidas Guibas, and Johannes Wallner. 2010. Geodesic patterns. *ACM Trans. Graph.* 29, 4, Article 43 (jul 2010), 10 pages. https://doi.org/10.1145/1778765.1778780

Helmut Pottmann, Alexander Schiftner, Pengbo Bo, Heinz Schmiedhofer, Wenping Wang, Niccolo Baldassini, and Johannes Wallner. 2008. Freeform surfaces from single curved panels. *ACM Trans. Graph.* 27, 3 (aug 2008), 1–10. https://doi.org/10.1145/1360612.1360675

Ahmad Rafsanjani and Katia Bertoldi. 2017. Buckling-Induced Kirigami. *Physical Review Letters* 118 (2017). Issue 8. https://doi.org/10.1103/PhysRevLett.118.084301

Ahmad Rafsanjani, Lishuai Jin, Bolei Deng, and Katia Bertoldi. 2019. Propagation of pop ups in kirigami shells. *Proceedings of the National Academy of Sciences* 116, 17 (2019). https://doi.org/10.1073/pnas.1817763116

Yingying Ren, Julian Panetta, Tian Chen, Florin Isvoranu, Samuel Poincloux, Christopher Brandt, Alison Martin, and Mark Pauly. 2021. 3D Weaving with Curved Ribbons. *ACM Trans. Graph.* 40, 4, Article 127 (jul 2021), 15 pages. https://doi.org/10.1145/3450626.3459788

Emmanuel Rodriguez, Georges-Pierre Bonneau, Stefanie Hahmann, and Mélina Skouras. 2022. Computational Design of Laser-Cut Bending-Active Structures. *Computer-Aided Design* 151 (2022), 103335. https://doi.org/10.1016/j.cad.2022.103335

Victor Romero, Mickaël Ly, Abdullah Haroon Rasheed, Raphaël Charrondière, Arnaud Lazarus, Sébastien Neukirch, and Florence Bertails-Descoubes. 2021. Physical validation of simulators in computer graphics: a new framework dedicated to slender elastic structures and frictional contact. *ACM Trans. Graph.* 40, 4 (2021). https://doi.org/10.1145/3450626.3459931

Madlaina Signer, Alexandra Ion, and Olga Sorkine-Hornung. 2021. Developable Metamaterials: Mass-Fabricable Metamaterials by Laser-Cutting Elastic Structures. In *Proceedings of the 2021 CHI Conference on Human Factors in Computing Systems* (, Yokohama, Japan,) *(CHI '21)*. Association for Computing Machinery, New York, NY, USA, Article 674, 13 pages. https://doi.org/10.1145/3411764.3445666

Oded Stein, Eitan Grinspun, and Keenan Crane. 2018. Developability of Triangle Meshes. *ACM Trans. Graph.* 37, 4, Article 77 (jul 2018), 14 pages. https://doi.org/10.1145/3197517.3201303

Seiichi Suzuki, Alison Martin, Yingying Ren, Tzu-Ying Chen, Stefana Parascho, and Mark Pauly. 2023. *BamX: Rethinking Deployability in Architecture through Weaving*. De Gruyter, Berlin, Boston, 207–220. https://doi.org/doi:10.1515/9783111162683-016

Josh Vekhter, Jiacheng Zhuo, Luisa F Gil Fandino, Qixing Huang, and Etienne Vouga. 2019. Weaving Geodesic Foliations. *ACM Trans. Graph.* 38, 4, Article 34 (jul 2019), 22 pages. https://doi.org/10.1145/3306346.3323043

A Wächter, Lorenz Biegler, Yi-dong Lang, and Arvind Raghunathan. 2002. IPOPT: An interior point algorithm for large-scale nonlinear optimization. (01 2002).

Johannes Wallner, Alexander Schiftner, Martin Kilian, Simon Flöry, Mathias Höbinger, Bailin Deng, Qixing Huang, and Helmut Pottmann. 2011. *Tiling Freeform Shapes With Straight Panels: Algorithmic Methods*. 73–86. https://doi.org/10.1007/978-3-7091-0309-8_5

Charlie Wang and Kai Tang. 2005. Optimal Boundary Triangulations of an Interpolating Ruled Surface. *Journal of Computing and Information Science in Engineering* 5 (12 2005). https://doi.org/10.1115/1.2052850

Katja Wolff, Roi Poranne, Oliver Glauser, and Olga Sorkine-Hornung. 2018. Packable Springs. *Computer Graphics Forum* 37, 2 (2018), 251–262. https://doi.org/10.1111/cgf.13358

Yunlan Zhang, Jingyi Yang, Mingchao Liu, and Dominic Vella. 2022. Shape-morphing structures based on perforated kirigami. *Extreme Mechanics Letters* 56 (2022). https://doi.org/10.1016/j.eml.2022.101857

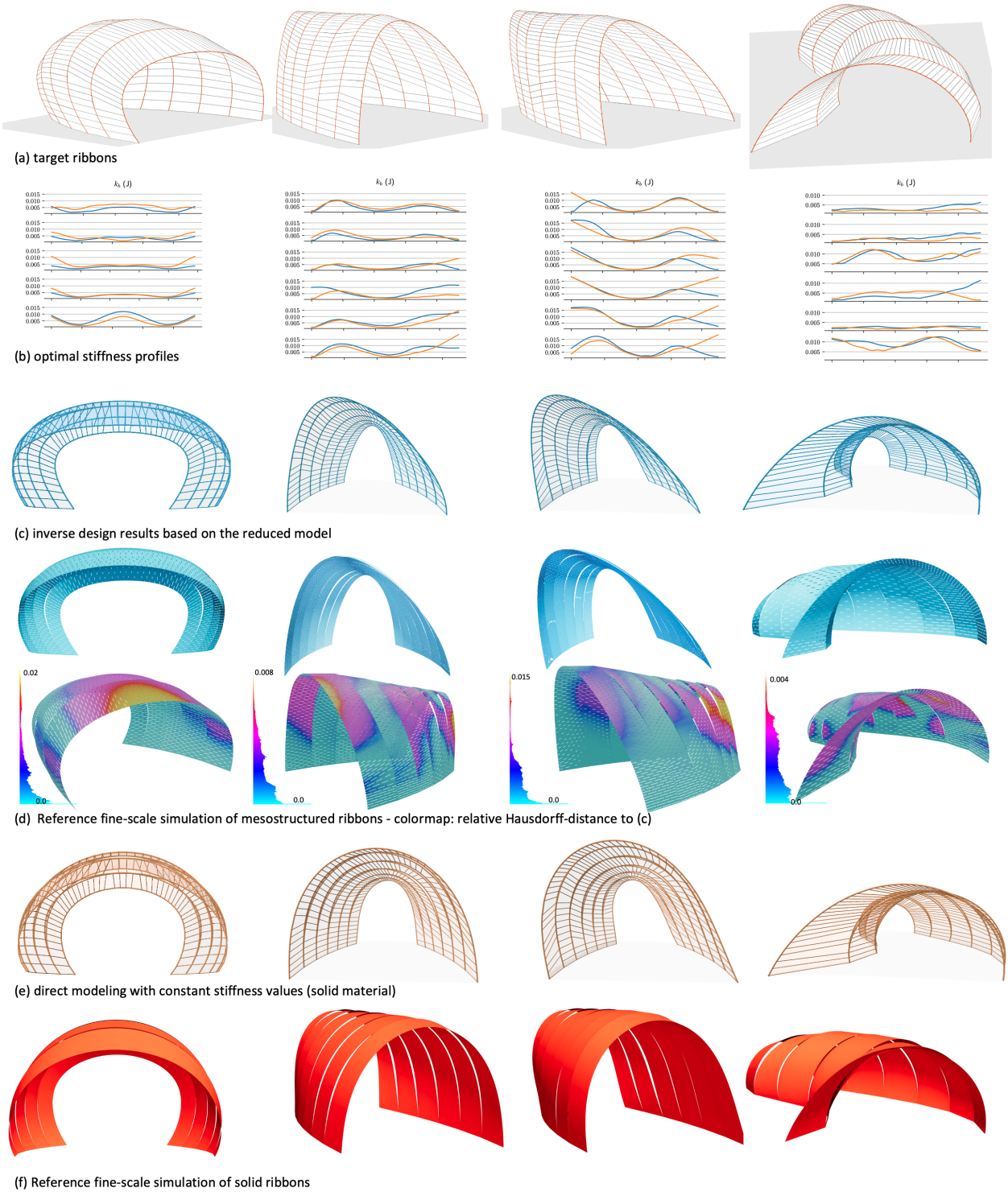

Figure 9: Representative results produced with our method. (a) Target ribbons are the developable quad strips with improved rulings. (b) Optimal stiffness profiles for each ribbon as output of the inverse design algorithm. (c) Reduced model with optimized stiffness values k_b from the inverse design algorithm. (d) Reference fine-scale simulation of the mesostructured ribbons, the color map indicates relative deviation to (c). (e) Reduced model with constant stiffness values (solid material). (f) Reference fine-scale simulation of the solid ribbons (with uniform constant stiffness).

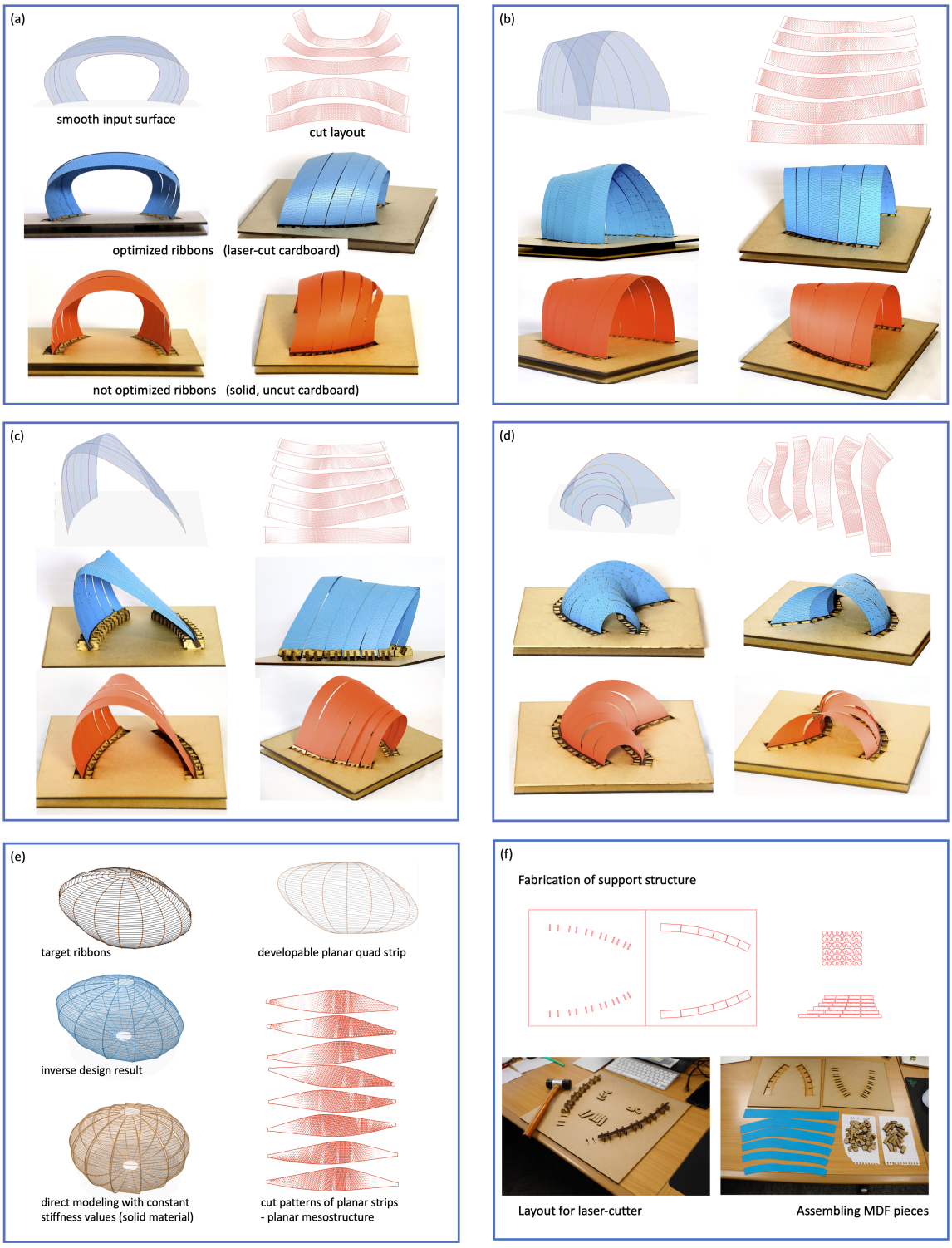

Figure 10: Fabrication of diverse physical models of cardboard clamped onto a MDF support. Results in (a)-(d) showcase the smooth freeform input surface, the computed layout of the mesostructured planar ribbons. The laser-cut patterned ribbons are assembled individually onto the support structure (blue cardboard) and can be compared to the input shape. For comparison, we fabricated the same ribbons from solid cardboard without the optimized pattern (red cardboard). The example in (e) demonstrates the ability of our method to serve for other models. (f) Fabrication of the support structure using the laser-cutter. The geometry of the individual pieces are computed in order to adapt to the different imposed boundary conditions for each model.